



Structural, magnetic and thermal characterization of Fe₅₀Se₅₀ powders obtained by mechanical alloying

Abdelhak Chebli^{1,2} · Abdelmalik Djekoun¹ · Joan Josep Suñol³ · Daniel Nižňanský⁴

Received: 26 March 2019 / Accepted: 30 August 2019 / Published online: 16 September 2019
© Akadémiai Kiadó, Budapest, Hungary 2019

Abstract

In this paper, Fe₅₀Se₅₀ alloy powders were synthesized from pure elemental powder by mechanical allowing. The structure, microstructure, morphology, chemical composition and thermal behavior at a function of milling times (0–39 h) were investigated by X-ray diffraction (XRD), scanning electron microscopy attached with energy-dispersive spectroscopy and differential scanning calorimetry (DSC). In addition, the interaction hyperfine and magnetic proprieties was examined by transmission Mössbauer spectroscopy (TMS) and thermomagnetic measurements (VSM) respectively. For milling times up to 6 h, the results of refinement of the X-ray diffraction pattern by MAUD software reveal the formation of the β-FeSe hexagonal, amorphous selenium and nanocrystalline α-Fe. The DSC curves show several exothermic and endothermic peaks associated with various phases' transitions such as the exothermic peak at 103 °C related to crystallization amorphous selenium. However, after prolonging the milling time to 39 h, the XRD shows the formation of α-FeSe phase tetragonal which has plenty of technological interests especially the superconductivity. The Mössbauer spectroscopy confirmed the formation the two-phase paramagnetic hexagonal β-FeSe and α-FeSe tetragonal, according to the XRD and DSC. Measurement of magnetization (VSM) displays that saturation magnetization (MS) decreases as the milling time increases.

Keywords FeSe alloys · X-ray diffraction · Nanostructured materials · Magnetic proprieties · Mechanical alloying

Introduction

The iron selenide, (FeSe) alloys, received great attention of researches due to its electrical, optical and magnetic properties [1, 2]; the Fe–Se alloys are usually structured in several crystalline forms, such as FeSe₂ that has an orthorhombic marcasite structure, the hexagonal Fe₇Se₈

phase, β-FeSe phase with hexagonal NiAs-type structure, α-FeSe phase with tetragonal PbO-like structure and monoclinic Fe₃Se₄ phase. The various structures give very interesting properties that make iron selenide a very promising alloy for applications in different fields in the industry especially in equipment for solar cells [3], superconductivity and in optoelectronics [4].

It is known that Fe–Se alloys can be prepared by various techniques, spray pyrolysis [5, 6], selenization of iron films [7], hydrothermal method [8], metal organic chemical vapor deposition [9], microwave synthetic method [10] and solid-state reaction [11]. Several researchers have developed Fe–Se alloys by mechanical allowing [12–15], because of the considerable difference between their melting temperature iron (1535 °C) and selenium (217 °C) which makes it difficult to get Fe–Se alloy structures at a precise ratio by these techniques. Among them, the mechanical alloying (MA) technique has advantage of simplicity, which is considered the most interesting useful tool for the development of nanostructured alloys from

✉ Abdelhak Chebli
chebli1976@yahoo.fr

¹ Laboratory of Magnetism and Spectroscopy of Solids (LM2S), University of Badji Mokhtar, Faculty of Science, B. P. 12, 23000 Annaba, Algeria

² High-School of Technological Education (ENSET), Skikda, Algeria

³ Departamento de física, Universitat de-Girona, Campus Montilivi, 17071 Girona, Spain

⁴ Department of Inorganic Chemistry, Faculty of Science, Charles University in Prague, Hlavova 8, 128-42 Prague 2, Czech Republic

elemental powders [16]; the materials obtained by this method are homogeneous and are in the form of powders, for that reason it is easy to industrialize by powders metallurgy. Because of repeated shocks and under the effect of forces, the powders are subjected to significant plastic deformation and are deformed, cold-welded and repeatedly fractured; the high-energy ball-milling technique is used for refining the microstructures and furthermore for activating chemical reactions between elements. The interdiffusion between elements can be facilitated by the creation of structural defects, where the repeated shocks between balls powders and the inner wall of the vial create numerous crystalline defects as grain boundaries, vacancies, interstitials and dislocations.

In this work, we aim to develop nanostructured powders of $\text{Fe}_{50}\text{Se}_{50}$ composition by mechanical alloying. Our select composition $\text{Fe}_{50}\text{Se}_{50}$ in this research is different from compositions investigated in the precedent papers. Therefore, effect of milling times (0–39 h) in structure, microstructure, thermal and magnetic properties of the $\text{Fe}_{50}\text{Se}_{50}$ powders was studied.

Experimental

Materials and methods

Elemental powders of Fe (99.98%, particle size $\sim 10 \mu\text{m}$) and Se (99.5%, particle size $\sim 10 \mu\text{m}$) were weighted and mixed in proportions corresponding to the nominal composition $\text{Fe}_{50}\text{Se}_{50}$ (at.%) and ball-milled at room temperature under argon atmosphere using a planetary ball mill (Fritsch Pulverisette 7). The ball-to-powder mass ratio was 10:1, and the rotation speed was 600 rpm. To avoid excessive heating during MA, each 30 min of MA was followed by a pause of 15 min. Phases identification and microstructure change (crystallite size, microstrains and lattice parameter and relative fraction) of milled powders were performed with X-Ray diffraction (XRD) using Panalytical X'pert powder diffractometer, with $\text{Cu K}\alpha$ radiation $\lambda = 0.15481 \text{ nm}$ in 2θ range 10° – 120° in Bragg–Brentano geometry.

The diffraction patterns were refined with the help of MAUD program [17]; the refinement is based on Rietveld method [18, 19]. The morphology and composition studies of the powders were examined by scanning electron microscopy (SEM) using DSM 96030 microscope attached with energy-dispersive spectroscopy (EDS). The thermal behavior of the milled powders was analyzed by using DSC with a PerkinElmer DSC7 under argon atmosphere, in the temperature range 30 – 600°C , at a heating rate of $10^\circ\text{C min}^{-1}$. The magnetic properties were carried out by using vibrating sample magnetometer (VSM) at room

temperature within an external field up to 10 KOe. Mössbauer spectroscopy is a method of studying hyperfine structures and magnetic properties of alloys based on iron. The Mössbauer spectra measurement was taken in the transmission mode with ^{57}Co diffused into an Rh matrix as the source moving with constant acceleration. The spectrometer (Wissel) was calibrated by means of a standard α -Fe foil, and the isomer shift was expressed with respect to this standard at 293 K. The samples were measured at room temperature. The fitting of the spectra was performed with the help of the NORMOS program by using Lorentzian profiles.

Results and discussion

Scanning microscopy and analyses

The variation in the morphology and composition of the particles during the mechanical alloying processes were followed by SEM/EDS. Figure 1 displays the morphology evolution of the $\text{Fe}_{50}\text{Se}_{50}$ powders before and after 3, 6, 12, 24 and 39 h of milling. As can be observed, different forms and morphologies of the particles are noted because of the repetition of the phenomena of fracture and welding during milling; for un-milled powders, the shapes are identical;

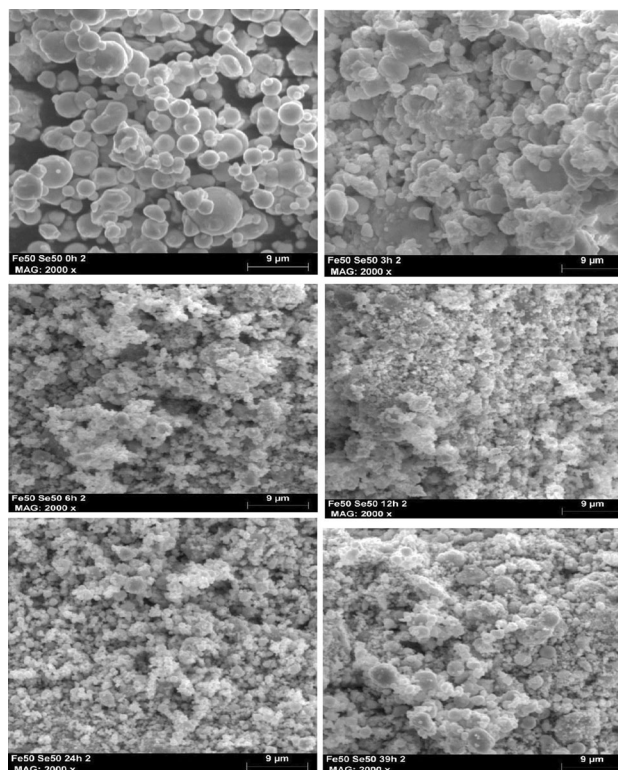


Fig. 1 SEM micrographs of $\text{Fe}_{50}\text{Se}_{50}$ powders prepared by mechanical alloying before and after different milling times

shape of some particles is irregular spheres. At 3 h of milling, we see the appearance of flattened form and large particles indicate that the welding phenomenon is dominant. In addition, some with a lamellar structure formed of alternating arrangement of Fe and Se layers. During milling and under the effect of repeated shocks between the particles and balls–balls and the inner wall of the vial, the lamellar structure is destroyed and refined and becomes small particles with different forms.

After 6 h of milling, the morphology of the powders looks small and homogeneous in size, we continue milling, the powders are subjected to repeated flattening, fracturing, and re-welding, and the particles will undergo more and more plastic deformation, which leads to a change in their morphology.

For all time of milling 12 h to 39 h, the milled powders show an agglomeration of the particles and fine particles with irregular contours or not homogeneous but with a size distribution; the competition between cold welding and fracturing among the powders is answerable for morphological changes that appear in them.

EDS analysis in (Fig. 2) shows energy peaks correspond to the elements in the sample Se and Fe; they are narrow and strong; the ratios 32.79: 29.86 and 33.37: 32.27 for 6 h and 39 h of the milling, respectively, show the homogeneity of the composition Fe₅₀Se₅₀. The EDS measurement reflects no contamination by milling tools and the presence of carbon due to the sample holder of the device. The oxygen is present only on the surface, not up to the reaction with Se or Fe.

X-ray diffraction and analyses

The structural evolution of the Fe₅₀Se₅₀ powders during milling process has been investigated by XRD (Fig. 3).

For powder un-milled mixture, the XRD pattern indicates the characteristic Bragg lines corresponding to pure iron α -Fe (card PDF No 00-006-0696 with lattice parameter $a = 0.2866$ nm and space group Im3m) and Se trigonal (card PDF No 00-006-0362 with lattice parameter $a = 0.4355$ nm and $c = 0.4948$ nm and space group P3221). After 3 h of milling, the crystalline peaks of selenium disappeared, indicating the formation of the amorphous selenium phase (partial amorphization); simultaneously, the peaks of the iron are broadened and their intensity decreases; however, the new diffraction peaks at $2\theta \sim 28^\circ, 30^\circ, 42^\circ, 50.50^\circ$ and 68° are corresponding to the formation of the phase β -FeSe (space group P63/mmc) hexagonal (NiAs-type). It is well known according to the literature that ball milling of pure trigonal or hexagonal selenium promotes a phase transformation from the crystalline to amorphous state after few hours of milling [20, 21] which could be responsible for the absence

of Se peaks; from the XRD analysis we can state that part of the Se is now amorphous, and the rest of the selenium is reacted with iron and the β -FeSe phase is formed. As milling progressed to 6 h, we can see evolution of diffraction peaks associated with β -FeSe; for milling times above 6 h, XRD pattern shows that the peaks began to broaden gradually and that intensity changes but inversely with increasing milling time. The broadening of the Bragg peaks and the decrease in their intensity are attributed to the decrease in grain size and to the internal strains induced by the high density of dislocations produced during the plastic deformations. In addition to the effect of heterogeneities chemicals, they are at a sufficiently scale fine; they cause local variations in lattice parameters and contribute to the broadening of peaks.

During the development of iron selenide system, various phases can be formed; according to Okamoto [22], the Fe–Se alloys system can structure in eleven crystalline different phases that complicates the identification of their structure after elaboration. The appearance of new diffraction peaks for powder milled at 39 h indexed to α -FeSe phase with tetragonal structure PbO-like (space group P4nm). The emergence the α -FeSe, explain the transition or decomposition some β -FeSe to α -FeSe, the phase transition during mechanical allowing can be explained by the changes of Gibbs free energy [23]. In addition, the tetragonal phase formed at higher temperatures, by comparison of the formation temperature of the hexagonal phase.

According to Grivel et al. [24], the formation of β -FeSe phase from Fe and Se requires the formation in succession of different phase's intermediate products and β -FeSe transforms into δ -FeSe around at 500 °C.

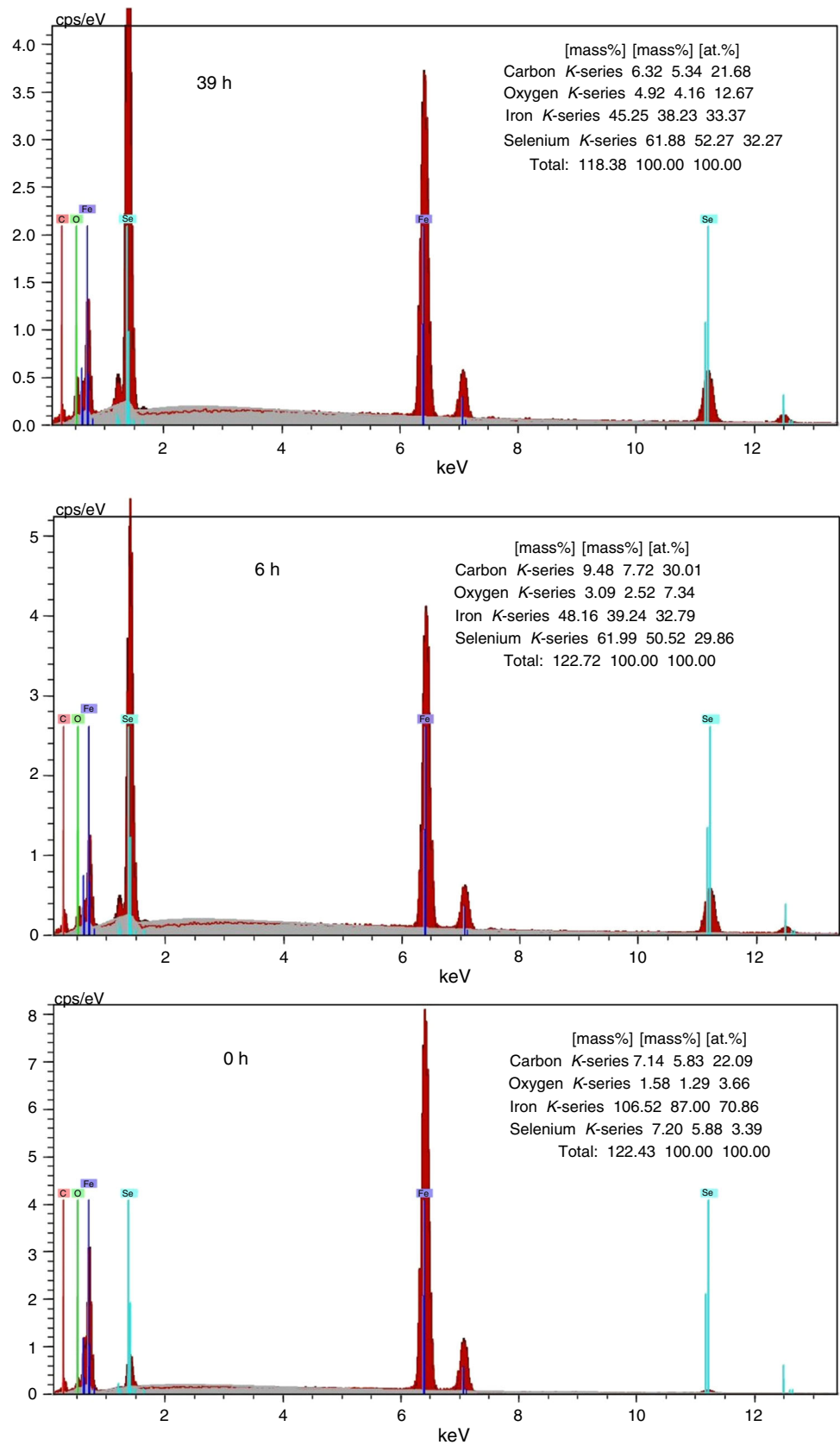
The tetragonal α -FeSe or β -FeSe phase-type PbO [25–29] is attracting the interest of scientists and researchers because of its outstanding electrochemical and magnetic properties [30, 31], especially after the discovery of its superconductivity feature [25].

X-ray diffraction (XRD) pattern analysis is not only applied for the identification of crystalline structures but also to determine the microstructural parameters of nanomaterials.

Figure 4 shows the Rietveld refinements of the experimental spectra of un-milled powders that have been made by introducing two phases: Fe (card PDF No 00-006-0696, with a lattice parameter $a = 0.2865$ nm) and Se trigonal (card PDF No 00-006-0362, with lattice parameter $a = 0.4355$ nm and $c = 0.4948$ nm).

The disappearance or emergence of Bragg peaks, for milling times 3 h at 6 h, is attributed to the formation of new phases. The milling process causes the accumulation of defects point and linear, such as vacancies; dislocations inside the particles lead to interdiffusion between elements

Fig. 2 EDS microanalysis corresponding to 0, 6, and 39 h milling



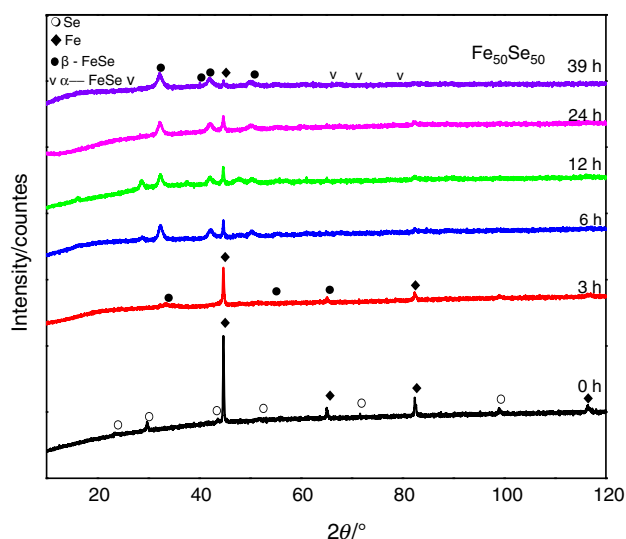


Fig. 3 XRD patterns of the Fe₅₀Se₅₀ powders milled for various times

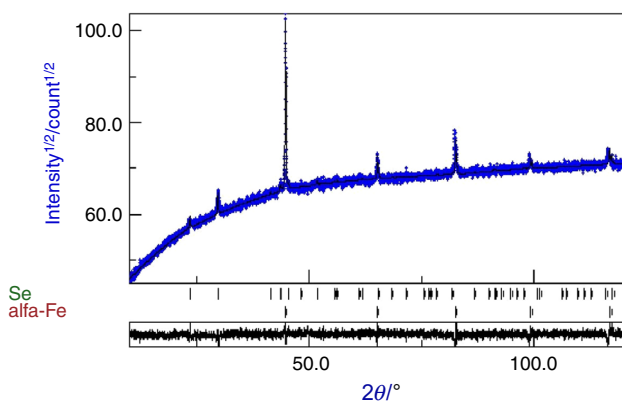


Fig. 4 Rietveld refinement of the XRD of powders Fe₅₀Se₅₀ un-milled experimental (dots) and calculated (full line) patterns are shown, difference is given below (Gof = 1.11)

at solid state, which lead to the phase formation. The best Rietveld refinements (Fig. 5) are obtained by amorphous-like phase Se, nanocrystalline Fe and β -FeSe hexagonal NiAs-type structure. For 39 h of milling, the Rietveld refinement (Fig. 6) is realized with two nanostructured phases, hexagonal β -FeSe and α -FeSe tetragonal and also the nanocrystalline Fe. Owing to the broadening of the diffraction peaks and the decrease in their intensity with the increase in milling time, which to an explanation by the reduction in the size of the grains or crystallite and the increase in the micro-deformation, for all the Rietveld refinement of spectra we used the model Popa rules.

The Rietveld refinement of Fe₅₀Se₅₀ mixtures permitted to well estimate the lattice parameters, average crystallite size $\langle D \rangle$, microstrains $\langle \sigma^2 \rangle^{1/2}$, and percentage of

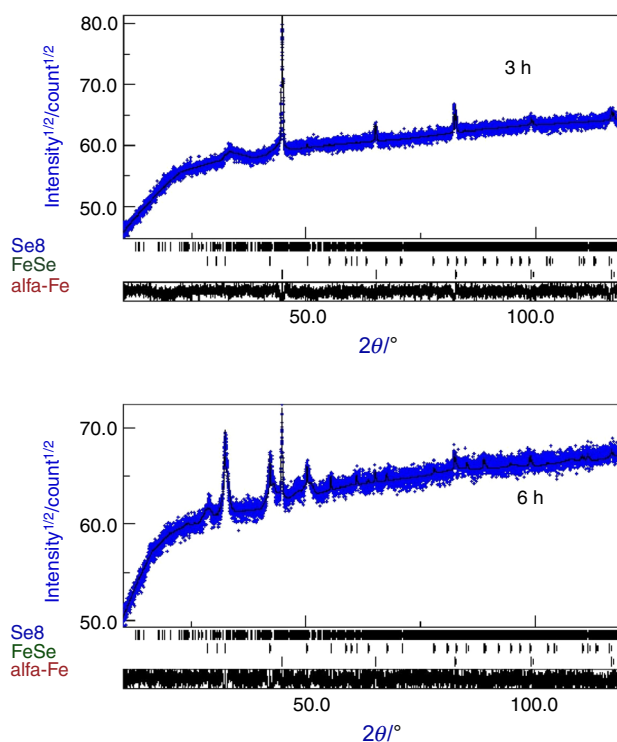


Fig. 5 Rietveld refinement of the XRD of powders Fe₅₀Se₅₀ milled 3 h and 6 h experimental (dots) and calculated (full line) patterns are shown, difference is given below (Gof = 1.13)

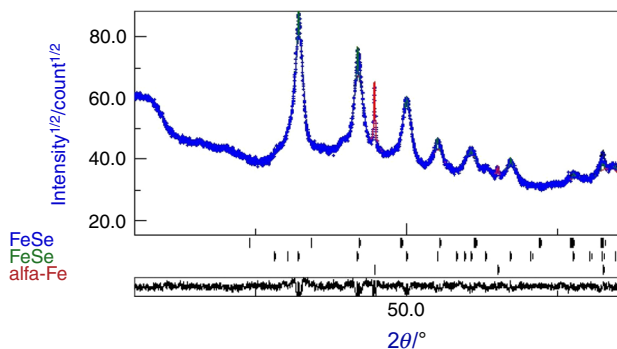


Fig. 6 Rietveld refinement of the XRD of powders Fe₅₀Se₅₀ milled 39 h experimental (dots) and calculated (full line) patterns are shown, difference is given below (Gof = 1.13)

phases formed as a function of the milling times, and (Table 1) grouped all the parameters that are deduced from the refinement. Our results are in agreement with the ones reported for the Fe–Se system elaborated by chemical vapor deposition [32], in which the superconducting tetragonal and hexagonal phases were formed. Moreover, Chen et al. [33] reported the formation of the tetragonal α -FeSe ($a = b = 3772 \text{ \AA}$ and $c = 5522 \text{ \AA}$) by solid-state reaction.

Table 1 Phases and structural parameters derived from Rietveld refinement of XRD patterns for Fe₅₀Se₅₀ for different milling times

Milling time/h	Phases	Lattice parameters/Å		$\langle D \rangle (\pm 5)/\text{nm}$	$\langle \sigma^2 \rangle^{1/2} (\pm 10^{-1})/\%$	Relative fraction/%
		$a (\pm 5.10^{-3})$	$b (\pm 5.10^{-3})$			
0	Se	$a = 4.3155$	$b = 4.4949$	~ 100		50
	Fe	$a = 2.8599$		~ 100		50
3	Se(amorphous)			~ 2	35	20
	Fe	$a = 2.8560$		76		38
	β -FeSe	$a = 3.6258$	$b = 5.8939$	55		42
6	Se(amorphous)			~ 2	56	04.01
	Fe	$a = 2.8561$		52		45.27
	β -FeSe	$a = 3.6285$	$b = 5.8521$	75		50.74
12	Fe	$a = 2.8627$		45	66	39.51
	β -FeSe	$a = 3.6285$	$b = 5.8521$	42		60.49
24	Fe	$a = 2.8628$		35	81	33.31
	β -FeSe	$a = 3.6237$	$b = 5.8709$	33		66.69
39	Fe	$a = 2.8630$		25	91	8.77
	α -FeSe	$a = 3.7720$	$b = 3.5220$	45		32.31
	β -FeSe	$a = 3.6396$	$b = 5.8607$	28		57.92

Harris et al. [34] and Zhang et al. [35] found that the two phases: tetragonal α -FeSe and the hexagonal β -FeSe, grow simultaneously.

The average crystallites size $\langle D \rangle$ decreases speedily during the first hours of milling, to attain a value of 25 ± 5 nm after 39 h of milling for the α -Fe. Thus, the average size of the crystallite obtained by MA depends on the milling conditions, especially the type of high-energy ball mill, the number and the diameter of the balls, the ratio mass of powders/balls, atmosphere of milling and the milling intensity.

On the other hand, the microstrain average ($\langle \sigma^2 \rangle^{1/2}$) changes in the same way as the size of the crystallite, but inversely they increase speedily during the first hours of milling and arrive at value of $0.9 \pm 0.1\%$ after 39 h of milling.

Mössbauer spectroscopy

The hyperfine interaction was investigated by transmission spectrometry Mössbauer using ⁵⁷Co source at room temperature. The fitting of the experimental spectra was performed by using NORMOS program [36] which operates Lorentzian profiles. Mössbauer spectra of samples Fe₅₀Se₅₀ at different milling times are presented in Fig. 7. For milling times 3 h and 24 h, the Mössbauer spectra contain two components. One component is sextet (subspectrum 1—sextet) which corresponds to the α -Fe with a mean hyperfine field (B_{hf}) equal to 33 T, and the intensity of

sextet decreases as the milling time increases. Another component (subspectrum 2—doublet) is a doublet which is paramagnetic with isomer shift $\delta = 0.43$ at 0.46 mm s⁻¹ and is attributed to phase β -FeSe [35]; their intensity increases with milling time increase, according to the work of Sklyarova et al. [37].

After prolonging the milling time at 39 h, the Mössbauer spectra present paramagnetic behavior with some trace of iron magnetic; it is composed of two doublets (subspectrum 2 and subspectrum 3), and one sextet (subspectrum 1—sextet), that the second doublet is corresponding to the tetragonal phase α -FeSe with isomer shift $\delta = 0.5400$ mm s⁻¹.

Blachowski et al. [38] reported that the isomer shift of the tetragonal α -FeSe phase, obtained from the direct reaction between Fe and Se, varies from 0.5476 (120 K) to 0.5640 (4.2 K). This is in accordance with our results. Furthermore, Mizuguchi et al. [39] showed a paramagnetic behavior of the tetragonal phase FeSe, with the doublet of isomer shift; δ or IS = 0.5380 mm s⁻¹.

In Table 2, we have illustrated the hyperfine parameters of all phases determined from Mössbauer spectra (site or subspectrum, isomer shift (δ), relative area, quadruple shift and hyperfine magnetic field B_{hf}). As the milling times increase, the relative fraction of the iron phase decreased and simultaneously the relative area of the phases formed via the milling process increases, in accordance with the results found by using XRD.

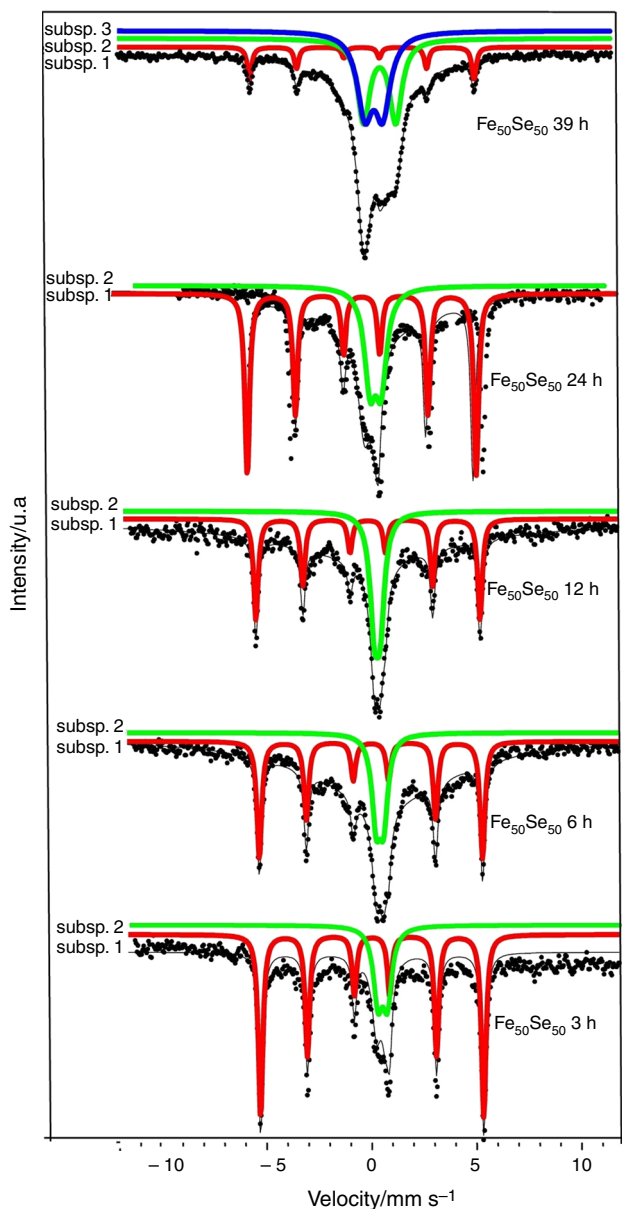


Fig. 7 Mössbauer spectra of Fe₅₀Se₅₀ powder mixtures milled for 3, 6, 12, 24 and 39 h

Magnetization measurements

The variation in the magnetic properties is due to the structure and microstructure, and they are ascribed to properties of nanomaterial, especially important grain boundaries surface area which contains a large fraction of atoms [40].

The magnetic hysteresis loops, taken at room temperature, for samples collected after 6, 12, 24 and 39 h of

milling are presented in Fig. 8. From 6 h up to 12 h of milling, all of them have similar shapes; the sigmoidal hysteresis cycles are usually observed in nanostructured powders with short magnetic domains. This is owing to the presence of structural distortions inside particles. The small cycles hysteresis losses the properties generally desired in soft magnetic materials. Figure 9 displays the variation of H_{CI} at all stage of milling. As can be seen, H_{CI} increases when milling time increases; the H_{CI} gradually increased with increasing mechanical alloying and peaked at $\sim 4.38 \pm 0.2 \text{ Ka m}^{-1}$. Increasing is maybe due to the decreasing crystallite and particle size, increasing lattice strain and redistribution of Fe and Se elements to facilitate phase change (*s*) during alloy formation. Figure 10 shows the variation of the saturation magnetization as a function of milling time, and a decrease in M_S from 0.85097 to 0.41530 emu g⁻¹ after 39 h of milling is observed.

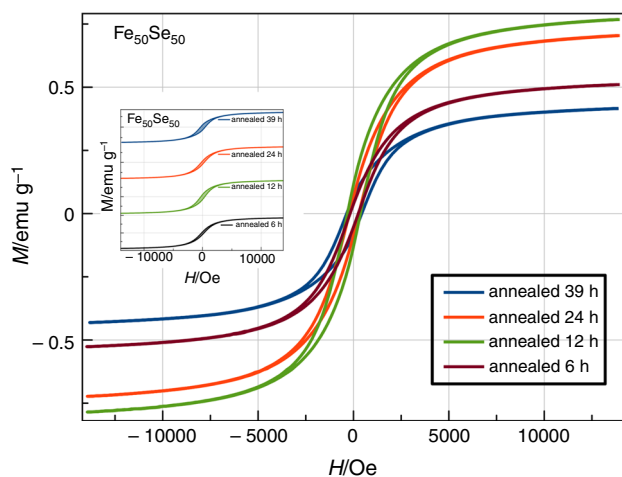
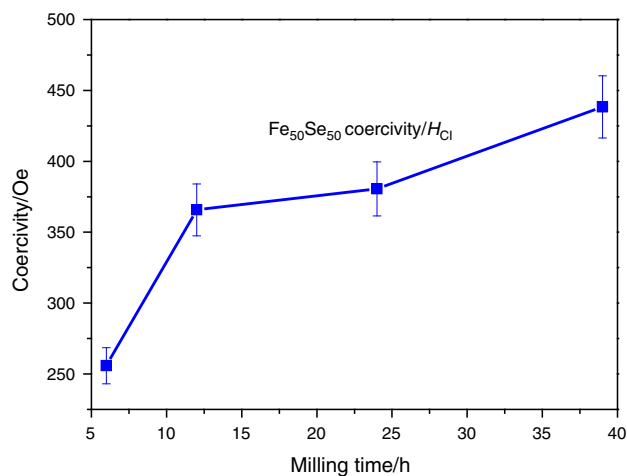
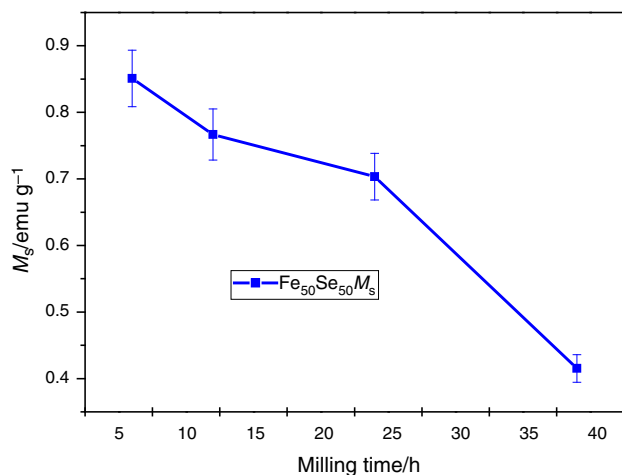
A recent research carried out on FeNi has shown that the saturation of magnetization (M_S) is dependent on the crystallite size and particle size [41], and the milling under argon atmosphere appeared to have a stronger influence on the (M_S), compared to the milling media [42].

DSC measurements

Figure 11 shows the DSC curves of powders milled at 3, 6, 12 and 39 h obtained by using heating rate 10 °C min⁻¹. The exothermic peaks located at 98–99 °C for powders milled 3 h and 6 h, respectively, correspond to the crystallization of amorphous selenium produced by the milling process. The formation of amorphous selenium phase in the Fe₅₀Se₅₀ mixture was confirmed by X-ray diffraction. This exothermic peak was also observed in the results of Chebli et al. [43]; however, the endothermic peak found at 54–55 °C is attributed to the glass transition of selenium (T_g), in agreement with the published literature [44]. Therefore, the peaks located at 150 °C and 280 °C for sample milled 3 h represent the structural relaxation of β -FeSe hexagonal and α -Fe nanostructured [43], confirming XRD results. The DSC curves also show an endothermic peak, at 221–224 °C, that corresponds to the selenium melting temperature, in close agreement with the temperature of the selenium, 217 °C. The same phenomena have been found by Liu et al. [45], showing the mixture of FeSe and FeSe_{0.7}Te_{0.3}, the emergence of an endothermic peak at 217–225 °C. At 6 h of milling, the exothermic stress relaxation process does not appear. This effect is probably

Table 2 The hyperfine parameters of all phases determined from Mössbauer spectra for $\text{Fe}_{50}\text{Se}_{50}$ powders for different milling times

Milling time/h		Isomer shift δ $\mp = 0.02/\text{mm s}^{-1}$	Quadrupole splitting ΔE_Q $\mp = 0.02/\text{mm s}^{-1}$	Hyperfine field B_{HF} $\mp = 0.02$	FWHM $\mp = 0.01/\text{mm s}^{-1}$	Relative area $\mp = 1/\%$	Phase
0	Subsp. 1	0,00	0,00	33,0	0,27	100	α -Fe
3	Subsp. 1	0,00	0,01	33,0	0,26	72	α -Fe
	Subsp. 2	0,43	0,45	N/A	0,52	28	β -FeSe
6	Subsp. 1	0,00	0,00	33,0	0,27	56	α -Fe
	Subsp. 2	0,43	0,35	N/A	0,71	44	β -FeSe
12	Subsp. 1	0,00	0,00	33,1	0,27	54	α -Fe
	Subsp. 2	0,43	0,55	N/A	0,67	46	β -FeSe
24	Subsp. 1	0,00	0,01	33,2	0,26	50	α -Fe
	Subsp. 2	0,44	0,28	N/A	0,49	50	β -FeSe
39	Subsp. 1	0,00	0,01	33,2	0,2	19	α -Fe
	Subsp. 2	0,46	1,53	N/A	0,71	39	β -FeSe
	Subsp. 3	0,54	0,84	N/A	0,88	42	α -FeSe

**Fig. 8** Hysteresis loop of $\text{Fe}_{50}\text{Se}_{50}$ samples milled for 3, 6, 12, 24 and 39 h**Fig. 10** Plots of intrinsic coercivity (H_{Cl}) at various milling times of $\text{Fe}_{50}\text{Se}_{50}$ powders**Fig. 9** Plots of saturation magnetization (M_s) at various milling times of $\text{Fe}_{50}\text{Se}_{50}$ powders

due to the stress release associated with the amorphous phase disappearance (between 3 and 6 h of milling the amorphous Se phase percentage is reduced from 20 to 4 at.%). For the milling time 39 h, the DSC curve shows an exothermic peak at 368 °C that attributed to the tetragonal FeSe phase, in agreement with the results obtained by Zhang et al. [46]. The endothermic peak at 480 and 482 °C, for milling time 12 h and 39 h, respectively, is related to decomposition of the β -FeSe phase. The DSC curve at 6 h of milling shows a broad endothermic peak at 520 °C, which is probably due to a solid-state transformation (β -FeSe transform to δ -FeSe) [12, 24]. The results obtained by the thermal analysis are consistent with those obtained by XRD and Mössbauer spectroscopy.

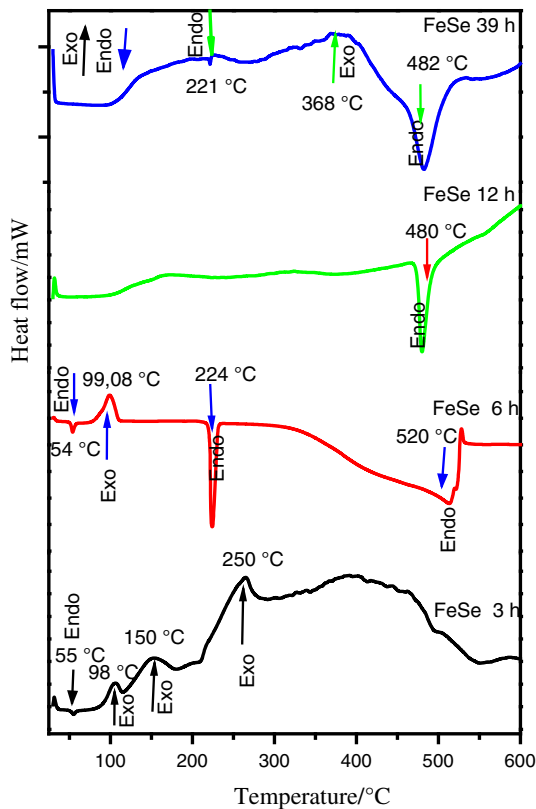


Fig. 11 DSC curves of Fe₅₀Se₅₀ powder mixtures milled for 3, 6, 12 and 39 h

Conclusions

The morphology, structure, thermal behavior, and magnetic and hyperfine properties of the iron selenide Fe₅₀Se₅₀ powders obtained by mechanical alloying have been studied by means of X-ray diffraction, scanning electron microscopy coupled with microanalysis (EDS), scanning calorimetry, vibration scanning manometer and Mössbauer spectroscopy, the mechanical alloying of elemental Fe and Se powders in high energy in Fe₅₀Se₅₀ composition resulted in the formation nanocrystalline alloys. The Rietveld refinement of XRD patterns for powders form 3 h and 6 h indicates Fe nanostructured, β -FeSe and Se amorphous. For 39 h, the XRD reveals FeSe tetragonal phase.

MS confirmed the presence of two phases, the tetragonal FeSe phase and the hexagonal phase with paramagnetic behavior in Fe₅₀Se₅₀ powders synthesized by high-energy mechanical alloy. The DSC curves show several endothermic and exothermic peaks, corresponding to glass transition, crystallization, melting and phases relaxation. The results extracted from XRD, DSC and MS are in very good mutual agreement.

Acknowledgements Financial support from High School of Technological Education (ENSET)–Skikda is acknowledged.

References

1. Wu XJ, Shen DZ, Zhang ZZ, Zhang JY, Liu KW, Li BH, Lu YM, Yoa B, Zahao DX, Li BS, Shan CX, Fan XW, Lin HJ, Yang CL. On nature of the carriers in ferromagnetic FeSe. *Appl Phys Lett*. 2007;90:112105.
2. Wu XJ, Zhang ZZ, Zhang JY, Ju ZG, Shan DZ, Li BH, Shan CX, Lu YM. Structural and electrical characterization of single tetragonal FeSe on Si substrate. *J Cryst Growth*. 2007;300(2):246–63.
3. Ouertani B, Ouertfelli J, Saadoum M, Bessais B, Ezzaouia H, Bernède JC. Transformation of amorphous iron oxide thin films predeposited by spray pyrolysis into a single FeSe₂ phase by selenisation. *Sol Energy Mater Sol Cells*. 2005;87(1–4):501–11.
4. Zhang S, Liu J, Feng J, Shao B, Li C, Zhang P. Optimization of FeSe superconducting tapes with different sheath materials and precursor powders. *J Supercond Novel Magn*. 2018;31–9:2747–51.
5. Ubale AU, Sakhare YS, Belkhedkar MR. Synthesis and characterization of spray deposited nanostructured FeSe thin films. *Mater Lett*. 2013;92:111–4.
6. Ubale AU, Skhare YS. Effet of substrate temperature on optical, structural and electrical properties of FeSe thin films deposited by spray pyrolysis technique. *J Phys Chem Solids*. 2013;74(10):1459–64.
7. Jin R, Zhao K, Pu X, Zhang M, Cai F, Yang X, Kim H, Zhao Y. Structural and photovoltaic properties of FeSe₂ films prepared by radio frequency magnetron sputtering. *Mater Lett*. 2016;179:179–81.
8. Sobhani A, Salavati-Niasari M. Synthesis and characterization of FeSe₂ nanoparticles and FeSe₂/FeO(OH) nanocomposites by hydrothermal method. *J Alloy Compd*. 2015;625(15):26–33.
9. Tao YR, Fan L, Wu ZY, Wu XC, Wang ZH. Synthesis and characterization of superconducting FeSe nanowires. *J Alloy Compd*. 2018;75:20–7.
10. Li ML, Yao QZ, Zhou GT, Fu SQ. Microwave-assisted synthesis of flower-like β -FeSe microstructure. *CrystEngComm*. 2010;12:3138–44.
11. Onar K, Yakinci ME. Solid state synthesis and characterization of bulk β -FeSe superconductors. *J Alloy Compd*. 2015;620(25):210–6.
12. Chebli A, Djekoun A, Sunol JJ, Niznansky D. Structural, thermal and hyperfine properties of Fe₇₅Se₂₅ powders prepared by mechanical alloying. *Mater Chem Phys*. 2018;217:477–85.
13. Feng JQ, Zhang SN, Liu JX, Ma XB, Zhang PX. Fabrication of FeSe superconducting tapes with high-energy ball milling aided PIT process. *Mater Lett*. 2016;170:31–4.
14. Xiaoting L, Zhiming G, Yongchang L, Zongqing M, Liming Y. Influence of premilling time on the sintering process and superconductive properties of FeSe. *IEEE Trans Appl Supercond*. 2012;22(6):7300105.
15. Ulbrich KF, Campos CEM. Nanosized tetragonal β -FeSe phase obtained by mechanical alloying: structural and microstructural, magnetic and electrical characterization. *RCA Adv*. 2018;8:8190–8.
16. Neikov OD. Handbook of non-ferrous metal powders technologies and application. 2nd ed. Amsterdam: Elsevier; 2019. p. 91–124.
17. Lutterotti L. MAUD program, CPD, Newsletter(IUCr). 2000. p P24.
18. Rietveld HM. A profile refinement method for nuclear and magnetic structures. *J Appl Cryst*. 1969;2:65–71.
19. Stewart RF, Bentley J, Goodman B. Generalized x-ray scattering factors in diatomic molecules. *J Chem Phys*. 1975;63(9):3786–93.
20. Campos CEM, De Lima JC, Grandi TA, Machado KD, Pizani PS. Structural studies of iron selenides prepared by mechanical alloying. *Solid State Commun*. 2002;123:179–84.

21. Elabbar AA, Abu-Sehly AA. Crystallization kinetics of amorphous selenium prepared by ball milling technique: evidence of three crystallization regimes. *Mater Chem Phys*. 2013;141(2–3):713–8.
22. Okamoto H. The Fe–Se (iron–selenium) system. *J Phase Equilib*. 1991;12:383.
23. Xia XJ, Huang FQ, Xie XM, Jiang MH. Preparation and superconductivity of stoichiometric β -FeSe. *Europhys Lett*. 2009;86:37008.
24. Grivel JC, Wulff AC, Zhao Y, Andersen NH, Bednarek J, Zimmermann MV. In situ observation of the formation of FeSe. *Supercond Sci Technol*. 2011;24:15007.
25. Hsu FC, Luo JY, Yeh KW, Chen TK, Huang TW, Wu PM, Lee YC, Huang YL, Chu YY, Yan DC, Wu MK. Superconductivity in the PbO-type structure α -FeSe. *PNAS*. 2008;105(38):1462–4.
26. Zahao PH, Yan W, Yang JY, Ham YL, Aldica G, Sandu V, Badica P, Nie JC. A simple fabrication of FeSe superconductors with high upper critical field. *J Supercond Novel Magn*. 2012;25:1781–5.
27. Zhang SN, Xiao BM, Liu JX, Jian FQ, Cheng SL, Ping X. Effect of high-energy ball milling time on the sintering process of FeSe superconductors. *Mater Sci Forum*. 2016;848:657–63.
28. Wu MK, Hsu FC, Yeh KW, Huang TW, Chang HH, Chen TK, Rao SM, Mok BH, Chen CL, Huang YL, Ke CT, Wu PM, Chang AM, Wu CT, Perng TP. The development of the superconducting PbO-type β -FeSe and related compounds. *Phys C*. 2009;469:340–9.
29. Zhang S, Feng J, Liu J, Shao B, Li C, Zhang P. Optimization of high-energy ball milling aided sintering process for FeSe superconductors. *IEEE Trans Appl Supercond*. 2017;27(5):1–4.
30. Takemura Y, Suto H, Honda N, Kukuno K, Saito K. Characterization of FeSe films prepared on GaAs substrate by selenization technique. *J Appl Phys*. 1997;81:5177.
31. Takemura Y, Honda N, Takahashi T, Suto H, Kakuno K. Isotropic magnetization in FeSe films on GaAs substrate. *J Magn Mater*. 1998;181:1319–20.
32. Hussain RA, Badshah A, La B. Fabrication, characterization and application of iron selenide. *J Solid State Chem*. 2016;243:179–89.
33. Chen N, Ma Z, Liu Y, Li X, Cai Q, Li H, Yu L. Influence of Sn doping on the phase formation and superconductivity of FeSe_{0.93}. *J Alloy Compd*. 2014;588(5):418–21.
34. Harris SB, Camata RP. Double epitaxy of tetragonal and hexagonal phases in the FeSe system. *J Cryst Growth*. 2019;514(15):54–9.
35. Zhang S, Shao B, Zahao G, Liu J, Feng J, Li C, Zhang P. Influences of Fe content on the fabrication of FeSe superconductors with high-energy ball milling aided sintering process. *J Alloy Compd*. 2017;729:823–7.
36. Brand RA. The NORMOS program is available from WISSEL GmbH. D-82319 Starnberg, Germany. *Nucl Instrum Methods Phys Res*. 1987;B28:398.
37. Sklyarova A, Lindén J, Tewari GC, Rautama EL, Kappinen M. ⁵⁷Fe Mössbauer study of a secondary phase in FeSe_{1-x} with a large quadrupole splitting. *Hyperfine Interact*. 2014;226:341–9.
38. Blachowski A, Ruebenbauer K, Zukrowski J, Perzewoznik J, Wojciechowski K, Stadnik M. Mössbauer spectroscopy evidence for the lack of iron magnetic moment in superconducting FeSe. *J Alloy Compd*. 2010;494:1–4.
39. Mizuguchi Y, Furubayashi T, Deguchi K, Tsuda S, Yamaguchi T, Takano Y. Mössbauer studies on FeSe and FeTe. *Phys C*. 2010;470:5339–83.
40. Khosravi S, Alizadeh M, Sharafi S, Maleh HK, Atar N. Structural, magnetic and electron transfer effect of Cr additive on Fe₆₅Co₃₅ nanopowder fabricated mechanical allowing. *Powder Technol*. 2015;279:262–8.
41. Ashokkumar T, Rajadurai A, Gopinath SCB. Saturation magnetization studies on iron-nickel ball milling nanopowders and spark plasma sintered specimens. *J Magn Magn Mater*. 2018;465:621–5.
42. Rathi A, Meka MV, Jayaraman TV. Synthesis of nanocrystalline equiatomic nickel-cobalt-iron alloy powders by mechanical alloying and their structural and magnetic characterization. *J Magn Magn Mater*. 2019;496(1):469–82.
43. Chebli A, Djekoun A, Boudinar N, Benabdeslem M, Otmani A, Bouzabata B, Sunol JJ. Synthesis and characterization of high-energy ball-milled nanostructured Fe₂₅Se₇₅. *JOM*. 2016;68(1):351–61.
44. de Lima JC, dos Santos VHF, Grandi TA. Structural study of the Zn–Se system by ball milling technique. *Nano Struct Mater*. 1999;11(1):51–7.
45. Liu G, Li J, Chen K. Reaction mechanism in fast combustion synthesis of superconducting FeSe and FeSe_{0.7}Te_{0.3}. *Acta Mater*. 2017;122:187–98.
46. Zhang S, Liu J, Feng J, Wang Y, Ma X, Li C, Zhang P. Fabrication mechanism of FeSe superconductors with high-energy ball milling aided sintering process. *Mater Chem Phys*. 2015;163(1):587–93.

Publisher's Note Springer Nature remains neutral with regard to jurisdictional claims in published maps and institutional affiliations.